Depletion kinetics in the photobleaching trapping reaction inside a flat microchannel

Sung Hyun Park,[1] Hailin Peng,[1] Raoul Kopelman,[1,*] Panos Argyrakis,[2] and Haim Taitelbaum[3,†]
[1]*Department of Chemistry, University of Michigan, Ann Arbor, Michigan 48109-1055, USA*
[2]*Department of Physics, University of Thessaloniki, 54124 Thessaloniki, Greece*
[3]*Department of Physics, Bar-Ilan University, Ramat-Gan 52900, Israel*
(Received 6 August 2004; revised manuscript received 23 November 2004; published 21 March 2005)

The diffusion-limited kinetics of the growth of a depletion zone around a static point trap in a thin, long channel geometry was studied using a laser photobleaching experiment of fluorescein dye inside a flat rectangular capillary. The dynamics of the depletion zone was monitored by the θ distance, defined as the distance from the trap to the point where the reactant concentration has been locally depleted to the specified survival fraction (θ) of its initial bulk value. A dimensional crossover from two dimensions to one dimension, due to the finite width of the reaction zone, was observed. We define a "parallel" and a "perpendicular" θ distance, along the slab long and short dimensions, respectively, and study their time development as a means to study the asymmetrical nature of the slab geometry. For all θ values, the crossover occurs concurrently for both θ distances when the depletion zone touches the boundary for the first time. We derive theoretical expressions for this geometry and compare them with the experimental data. We also obtain important insight from the ratio of the reactant concentration profiles in the parallel and perpendicular directions. Exact enumeration and Monte Carlo simulations support the anomalous depletion scaling results. Nevertheless, the crossover time (τ_c) is still found to scale with the width (W) of the rectangular reaction zone as $\tau_c \sim W^2$, as expected from the basic Einstein diffusion law.

DOI: 10.1103/PhysRevE.71.031107 PACS number(s): 82.50.−m, 82.20.−w, 05.40.Jc

I. INTRODUCTION

In a series of recent papers [1–3] we have addressed the issue of the anomalous depletion zone of Brownian particles around a static trap (point trap and finite-sized trap), perfect and imperfect, in one and two dimensions, as a means to study photobleaching and other "trapping" dynamics in low dimensions. Because of the sensitivity of anomalous kinetics to the spatial dimensionality of the system [4–15], we extend, in the current work, our earlier studies to study the typical geometry of a flat microchannel.

It has been well established that the kinetic laws for reactions in a diffusion-limited environment are considerably different from the conventional rate laws, due to the spatial correlations of the reactants, originating from the inefficiency of the diffusive mixing [4–12]. One of the simple cases of the diffusion-limited reaction is the trapping reaction $A+T\rightarrow T$, where T is a static trap and A is a diffusing species that may be annihilated upon collision with the trap, depending on the trap strength. The trapping reaction in a diffusion-limited environment is closely related to a variety of processes, such as electron-hole trapping and recombination, exciton trapping, soliton-antisoliton recombination, phonon upconversion, free radical scavenging, electrolysis, etc. In many cases, the process occurs in low dimensional systems such as pores, filaments, microcapillaries, or thin molecular wires [6]. The occurrence of A-T reactions creates a zone of depletion around the trap, which is a form of self-segregation of reactants. The growth of the depletion zone in the trapping reaction in low dimensions leads to anomalous kinetics for a variety of dynamic quantities. For example, the nearest neighbor distance was found to increase asymptotically as $t^{1/4}$ in one dimension (1D) [7,8] and $(\ln t)^{1/2}$ in two dimensions (2D) [9–11], while the trapping reaction's global rate was shown to decrease asymptotically as $t^{-1/2}$ in 1D [7,8] and $(\ln t)^{-1}$ in 2D [10,11], where t is the time elapsed since switching-on of the trap.

A quantity relevant for the description of the depletion zone is the so-called θ distance (r_θ), which is the distance from the trap to the point where the local concentration of surviving A particles, $c(r,t)$, reaches the specified survival fraction θ ($0\leqslant\theta\leqslant 1$) of its value in the bulk c_0 [9,10], i.e.,

$$c(r_\theta,t)=\theta c_0. \tag{1}$$

The θ distance has been shown, by theory [10] and experiment [1], to increase asymptotically as $t^{1/2}$ in 1D. The $t^{1/2}$ dependence in 1D is explained on the basis of diffusion of particles towards the trap. In two dimensions, though, the θ distance has been shown theoretically to behave in an anomalous manner, exhibiting a nonuniversal $t^{\theta/2}$ behavior in the long-time limit [9–11]. These results have been recently confirmed experimentally [1–3]. In [1–3] we have used a Hele-Shaw cell, 150 micron thick, in order to produce both one-dimensional ("line trap" [1]) and two-dimensional ("point trap" [2,3]) systems. This experimental design allowed us to measure the temporal changes in the spatial distribution of the reactants at the trap vicinity, and then to analyze the dynamics of the depletion zone through the θ distance measure. In addition, an interesting short-time behavior has been observed, in particular in two dimensions. The effects of the finite size and the shape of the trap have been studied as well.

*Electronic mail address: kopelman@umich.edu
†Electronic mail address: haimt@mail.biu.ac.il

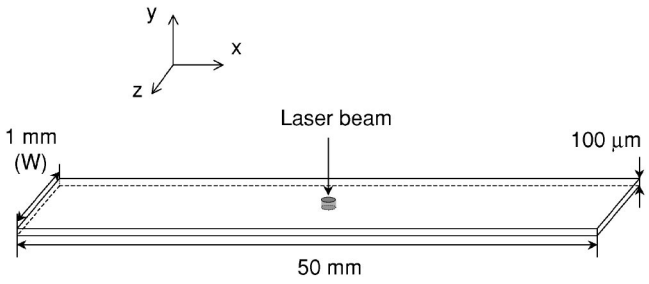

FIG. 1. A schematic slab geometry with a point trap.

In this paper we study the depletion zone formed in two-dimensional slablike geometry for a single point trap, located in the middle of the slab. Such a confined geometry interpolates between 2D and 1D dimensionalities, thus allowing one to examine the dimensional crossover behavior.

The experimental manifestation of the slab geometry is a flat capillary (Fig. 1). The capillary is 50 mm long, of the order of 1 mm wide, and 0.1 mm (100 μm) thick. This size suggests that this capillary is primarily a quasi-one-dimensional object. However, since the width and the thickness differ by an order of magnitude in size, this capillary can be considered as a quasi-two-dimensional object, thus allowing us to study experimentally a possible dimensional crossover between the local two-dimensional geometry and the one-dimensional dominant shape of the capillary.

It should be noted that, in such a geometry, careful consideration should be given to the proper definition of the depletion zone (i.e., the θ distance), as one no longer has either the radial symmetry of the two-dimensional case, or the trivial geometry of the one-dimensional case. We have therefore measured the depletion zone along the two extreme possibilities. The first is *parallel* to the slab length and the other is *perpendicular* to this direction, which is the shortest possible direction, limited by the slab width size.

We have also looked at the shape of the profiles along these two orthogonal lines, in order to gain more insight on the asymmetrical nature of the diffusion in the presence of a point trap in the slab geometry. In particular, we have studied the ratio of these quantities and its dimensional crossover characteristics.

The paper is organized as follows: In Sec. II we describe the experimental methodology and the experimental results. In Sec. III we derive theoretical expressions for this system and compare them with the experimental data. In Sec. IV we present simulation data performed using two methods: Monte Carlo simulations and exact enumeration. Finally, we summarize the work in Sec. V.

II. EXPERIMENT

A. Methods

The experiment is the laser photobleaching of fluorescein dye molecules in an aqueous solution. The fluorescein diffuses in water with a diffusion coefficient of 4.37×10^{-10} m^2 s^{-1} [16]. The photobleaching reaction occurs within the laser focus, inside a thin, long rectangular glass capillary with dimensions 0.1 mm $\times$ 1 mm $\times$ 50 mm (Fig. 1).

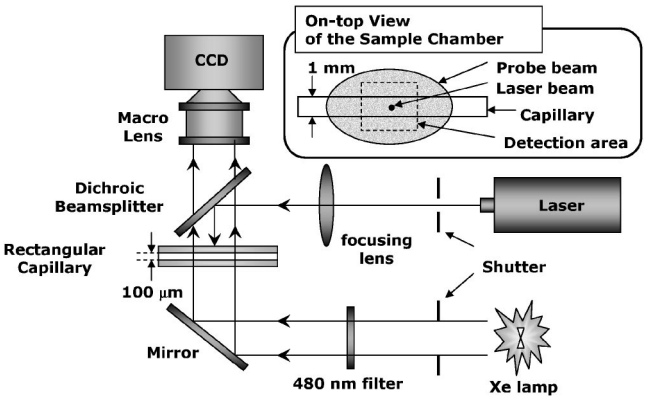

FIG. 2. A schematic diagram of the experimental setup.

An aqueous solution of fluorescein was prepared in a phosphate buffer solution at *p*H 8.5 with a concentration of 3.6×10^{-5} M. Spectroscopic grade fluorescein dye was purchased from Aldrich and used without further purification. The buffer solution was used to increase the solubility of the fluorescein as well as to prevent any potential *p*H change of the solution during the photobleaching process. The aqueous fluorescein solution was injected into the capillary using a glass pipette. After the sample injection, the capillary was sealed with epoxy to prevent the evaporation of the sample solution during the data acquisition.

The schematic diagram of the experimental setup is shown in Fig. 2. A 488-nm laser beam out of an air-cooled Ar-ion laser (Ion Laser Technology, model no. 5490AWC-0), introduced from above the capillary, is focused at the center of the rectangular capillary to photobleach the dye molecules, producing a circular trap cross section on the 1 mm $\times$ 50 mm sample plane. The output power of the laser beam was 16 mW and the diameter of the beam at the focus on the sample plane was approximately 65 μm. Another light source at 480 ± 5 nm with approximately 1 in diameter, a Xenon arc lamp (Sutter Instrument Company, model: Lambda DG-4), located below the capillary, was used to probe the progress of the photobleaching. The power density of the probe beam is less than 0.1% that of the photobleaching laser beam, so the effect of photobleaching by the probe beam is negligible during the typical time scale of the experiment. Further protection of the sample from the probe beam was provided by two mechanical shutters installed in front of the light sources. The two shutters operate out of phase to each other, so that either the photobleaching beam or the probe beam illuminates the sample alternately in time, which minimizes the exposure of the sample to the probe beam.

The images of fluorescence emission from the sample were collected during the photobleaching at different times, using a CCD camera (Roper Scientific, model: Photometrics Cool Snap ES) equipped with a macro lens (Nikon, AF Macro 60 mm f2.8, 1:1). The image is 4.5×3.3 mm^2 in size, with a 695×518 pixel resolution and a 14-bit intensity resolution. This produces an approximately 6.5 μm/pixel spatial resolution. Typical integration time of the CCD was 300 ms for each image. The dye molecule becomes invisible from the detector when photobleached, resulting in the intensity drop in the fluorescence image.

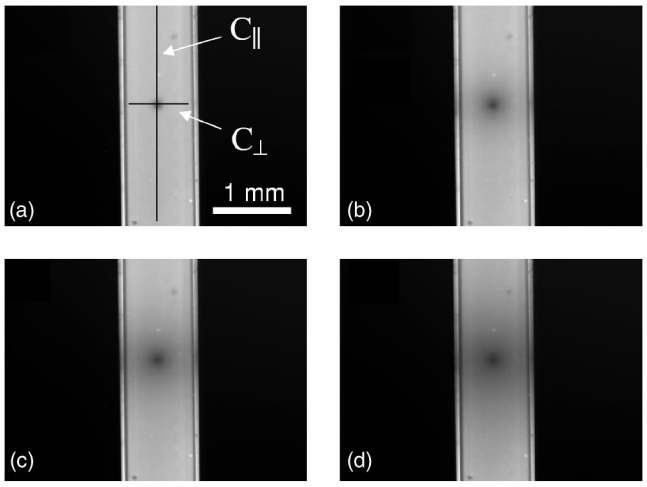

FIG. 3. Fluorescence images from a point trap experiment at selected times of (a) 1 s, (b) 160 s, (c) 500 s, and (d) 1500 s, showing the progress of the photobleaching of an aqueous fluorescein solution inside a rectangular capillary. The bright vertical band represents the capillary and the dark region in the middle of the capillary shows the growth of the depletion zone around the laser phototrap in time.

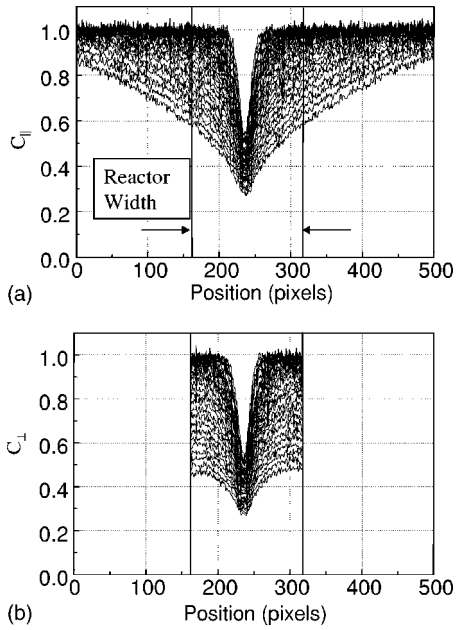

FIG. 4. Profiles of the concentration fractions of reactants in time from a point trap experiment, along a pixel line (a) parallel, and (b) perpendicular to the channel, as defined in Fig. 3(a). The time range is from 1 s to 1900 s. The solid vertical lines represent the width of the capillary channel.

The progress of the photobleaching was monitored up to 1900 s in the typical experiment. The entire experiment is performed at room temperature. A similar experimental setup has been used recently to study the trapping reactions in effective 1D and 2D [1–3].

B. Results

Figure 3 shows a series of the fluorescence images at $t=1$ s, 160 s, 500 s, and 1500 s from a point trap experiment inside a rectangular capillary, illustrating the progress of the photobleaching in time. The bright vertical band in the middle of the image represents the reaction channel in the rectangular capillary. The dark region, growing in the middle of the reaction channel, reflects the depletion zone developing around the phototrap. We note that the radial symmetry of the concentration profile, observed in normal 2D point trap systems [2,3], does not exist in the current rectangular capillary system, due to the narrow width of the reaction channel. Hence, to examine the possible directional dependence of the growth of the depletion zone around the point trap, we extracted the fraction profiles of the local reactant concentrations along the two separate pixel lines, parallel ($C_{\|}$) with and perpendicular ($C_{\perp}$) to the channel, through the center of the phototrap, as shown in Fig. 3(a). No evidence for convection was seen, and the comparison of the results below with purely diffusional theoretical models is consistent with a convectionless reaction process.

The time evolutions of the two fraction profiles, $C_{\|}$ and $C_{\perp}$, along the two pixel lines, are shown in Fig. 4. The time ranges for both profiles in Fig. 4 are identical, from 1 s up to 1900 s. Two solid vertical lines in each plot indicate the width of the rectangular capillary. A close comparison between the two profiles shows that they indeed develop differently in time, as expected from the absence of a radial symmetry for this geometry. For example, the $C_{\|}$ decreases to just below 0.6 at the distance corresponding to the width of the capillary during the given time period of 1900 s, while the $C_{\perp}$ decreases to as low as ~ 0.45 at the boundary of the capillary during the same period of time.

The reason for this behavior in the perpendicular direction near the boundary is the effect of a diminished supply of diffusing particles near the boundary. Qualitatively, the particle concentration in a region at a certain time is determined by the combination of the flux into and the flux out of the region at that time. With a trap in the middle of a space having a dimension lower than 3, the flux into a region, located in the interior part of the space outside the trap, is smaller than the flux out of the region at a given time. This is because the particles can diffuse out of the region freely, while the trapping process permits fewer particles to diffuse back into the region. This results in a concentration gradient around the trap and the development of a "normal" concentration profile. However, when the region is at or near the boundary of the space, the flux out of the region towards the trap is the same as without the boundary, while the flux into the region is reduced further than without the boundary, because there is less or no reservoir space to supply particles between the region and the boundary. This results in a faster drop in the particle concentration near the boundary.

Each θ distance was measured directly from the profiles in Fig. 4, and is presented in Fig. 5 as a function of time. The θ distance in the parallel and perpendicular direction is denoted as $r_{\theta}^{\|}$ and $r_{\theta}^{\perp}$, respectively. The solid straight lines correspond to the theoretical asymptotic slope of $\frac{1}{2}$ for 1D and the dashed straight lines represent the theoretical slopes of $\theta/2$ for 2D. The boundary of the capillary width is located

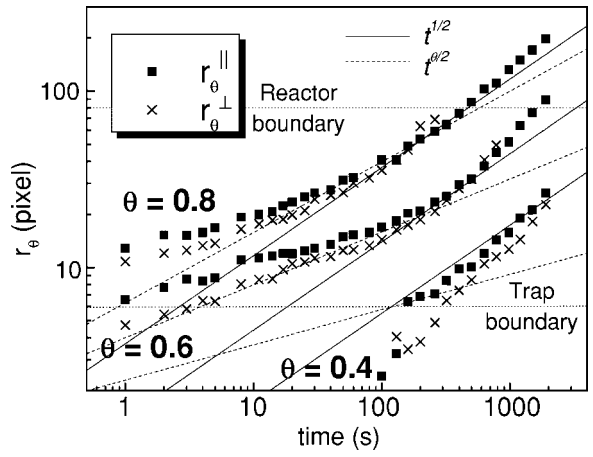

FIG. 5. The θ distance vs time for $\theta=0.4$, 0.6, and 0.8 from a point trap experiment. The solid squares ($r_\theta^{\parallel}$) represent the θ distance measured from Fig. 4(a) and crosses ($r_\theta^{\perp}$) from Fig. 4(b). The $r_\theta^{\parallel}$ and $r_\theta^{\perp}$ demonstrate a similar time scaling behavior for a given θ value until they reach the boundary of the capillary, after which $r_\theta^{\parallel}$ continues to grow while $r_\theta^{\perp}$ simply vanishes.

at a distance of ~77 pixels from the trap center, and the trap radius is ~5 pixels, as can be obtained using the conversion factor of 6.5 μm/pixel described in the above Methods section; both are indicated by dotted horizontal straight lines in Fig. 5. An immediately noticeable feature in Fig. 5 is that $r_\theta^{\parallel}$ and $r_\theta^{\perp}$ for a given θ value follow very similar dynamic pathways for most times. This is since the difference in their concentration profiles occurs only near the slab boundary, as pointed out earlier. Specifically, at $\theta=0.6$ and 0.8, both $r_\theta^{\parallel}$ and $r_\theta^{\perp}$ follow the intermediate-time behavior observed before in 2D [2,3], characterized as being slower than the asymptotic scaling of $t^{\theta/2}$, during the initial ~200 s. In the case of $\theta=0.4$, one can see the typical early-time, high slope inside the trap domain, which is also consistent with the previous study [2,3].

At around 300 s, both $r_\theta^{\parallel}$ and $r_\theta^{\perp}$, still coupled together, start to deviate from the 2D behavior, crossing over into a higher slope regime, seemingly approaching the 1D-like behavior at the long-time limit. This result indicates that the dynamics of the growth of the depletion zone goes through a dimensional crossover from an early-time 2D behavior to a long-time 1D behavior in both parallel and perpendicular directions in the rectangular capillary. The dimensional crossover is induced by the geometric constraint of the reaction space. After a slow growth of the depletion zone in the early-time range, the long and narrow channel shape of the rectangular capillary drives the depletion zone to grow at the faster 1D rate, once the geometric constraint from the narrow width of the capillary takes over. The faster concentration decay along the perpendicular direction near the boundary of the capillary, due to the diminished supply of reactant, discussed above, appears to have little effect on the overall dynamics of the θ distance. Its effect seems to be limited to the close proximity of the reactor boundary, where $r_\theta^{\perp}$ becomes bigger than $r_\theta^{\parallel}$ for $\theta=0.6$ and 0.8 in Fig. 5.

We also note that the deviation of the θ distance from the 2D pathway starts to set in at ~300 s, although the θ distances for all three θ values are still far away from the boundary at this time. In other words, the θ distance seems to "feel" the boundary of the reaction space well before it actually reaches this boundary. This is equivalent to the "reservoir" depletion effect discussed above. Once the θ distance actually reaches the boundary of the capillary, $r_\theta^{\parallel}$ continues to cross over to a high-slope, 1D-like behavior, while $r_\theta^{\perp}$ simply vanishes. It is somewhat surprising that $r_\theta^{\parallel}$, which has no direct contact with the boundary over the entire process, changes the dynamics from 2D to 1D almost simultaneously with $r_\theta^{\perp}$, which has a direct interaction with the boundary. It seems to imply that the boundary information is communicated between $r_\theta^{\parallel}$ and $r_\theta^{\perp}$ in real time. Actually, the higher parallel concentration profile compensates for the decreased perpendicular profile.

III. THEORY

The slab geometry is sketched in Fig. 1. The length is measured along the long coordinate x, and the width coordinate is z, ranging from $z=-W/2$ to $z=+W/2$ (W being the total width of the slab). The trap is located at $(x,z)=(0,0)$.

The analytical solution for this problem is based on the solution for diffusion inside an infinite three-dimensional region bounded by two parallel planes at $z=0$ and $z=W$, subject to a unit instantaneous source of particles at a given point (x_0,y_0,z_0) at time $\tau=0$ [17]. Assuming that the two boundaries satisfy reflecting boundary conditions, i.e., particles that reach these boundaries are reflected back inside the slab, the concentration profile of the particles anywhere inside the slab at time τ, is given by [17]

$$p(x,y,z;\tau)=\frac{1}{8(\pi D\tau)^{3/2}}e^{-(x^2+y^2)/4D\tau}\sum_{n=-\infty}^{+\infty}\left[e^{-(2nW+z_0-z)^2/4D\tau}+e^{-(2nW-z_0-z)^2/4D\tau}\right]. \quad (2)$$

For a two-dimensional region with symmetrical boundaries around a source at $z_0=0$, i.e., boundaries at $z=(-W/2,W/2)$, the y coordinate is omitted and the expression (2) reduces to

$$p(x,z;\tau)=\frac{1}{4\pi D\tau}e^{-x^2/4D\tau}\sum_{n=-\infty}^{+\infty}\left[e^{-[(2n+1)W-z]^2/4D\tau}+e^{-(2nW-z)^2/4D\tau}\right]. \quad (3)$$

In order to account for the cumulative effect of a continuous source up to time t, one must consider a continuous sequence of instantaneous sources at all times in the interval $[0,t]$. This is equivalent to integrating with respect to the time variable τ of Eq. (3),

$$p(x,z;t)=A(x,z;t)\int_0^t\frac{1}{4\pi D\tau}e^{-x^2/4D\tau}\sum_{n=-\infty}^{+\infty}\left[e^{-[(2n+1)W-z]^2/4D\tau}+e^{-(2nW-z)^2/4D\tau}\right]d\tau, \quad (4)$$

where an amplitude function $A(x,z;t)$ has been introduced in order to be able to normalize the result in accordance with

the boundary conditions of our two-dimensional trapping system. Interchanging the order of summation and integration, we obtain

$$p(x,z;t) = A(x,z;t) \sum_{n=-\infty}^{+\infty} \int_0^t \frac{1}{4\pi D\tau} e^{-x^2/4D\tau} \left[e^{-[(2n+1)W - z]^2/4D\tau} + e^{-(2nW - z)^2/4D\tau} \right] d\tau. \quad (5)$$

The integral in Eq. (5) can be solved exactly in terms of the exponential integral function $\mathrm{Ei}(y)$, defined as

$$\mathrm{Ei}(y) = \int_y^\infty \frac{e^{-u}}{u} du. \quad (6)$$

The solution for a continuous point source in two dimensions is then

$$p(x,z;t) = A(x,z;t) \sum_{n=-\infty}^{+\infty} \frac{1}{4\pi D} \left[\mathrm{Ei}\left(\frac{x^2 + [(2n+1)W - z]^2}{4Dt} \right) + \mathrm{Ei}\left(\frac{x^2 + (2nW - z)^2}{4Dt} \right) \right]. \quad (7)$$

We now use this result to obtain the appropriate expression for the concentration profile of the diffusing particles in the same geometry but in the presence of a continuous sink (trap) instead of a source. This expression, which will be denoted by $P(x,z;t)$, should be normalized so that there are no particles at the trap boundary, while there is a certainty to find particles far away from the trap. This condition, which formally reads

$$P(x,z;t) = \begin{cases} 0, & (x,z) = (0,0), \\ 1, & x \gg 1 \text{ or } z \gg 1 \end{cases} \quad (8)$$

implies that the final, normalized expression for the concentration profile $P(x,z;t)$ is

$$P(x,z;t) = 1 - \frac{\sum_{n=-\infty}^{+\infty} \left[\mathrm{Ei}\left(\frac{x^2 + [(2n+1)W - z]^2}{4Dt} \right) + \mathrm{Ei}\left(\frac{x^2 + (2nW - z)^2}{4Dt} \right) \right]}{\sum_{n=-\infty}^{+\infty} \left[\mathrm{Ei}\left(\frac{x^2 + [(2n+1)W - z]^2}{4Dt} \right) + \mathrm{Ei}\left(\frac{x^2 + (2nW - z)^2}{4Dt} \right) \right]_{(x,z)=\text{origin}}}, \quad (9)$$

where the denominator of the right-hand-side term is just the reciprocal of the normalization factor $A(x,z;t)$ introduced earlier, and is based on the numerator evaluated at the origin. This expression fulfills the boundary conditions of Eq. (8). In fact, due to the singularity of the Exponential Integral function $\mathrm{Ei}(y)$ at the origin $y=0$, substituting $(x,z)=(0,0)$ will cause the expression to diverge at the $n=0$ term. Therefore, one must introduce a cutoff at some finite size of the point trap. In further investigation we will use $(x,z)=(1,1)$ as the cutoff boundary for numerical calculations (in units corresponding to pixels).

The nature of the expression (9) can be best understood through the expansion of the exponential integral function, given as

$$\mathrm{Ei}(y) = -\gamma - \ln(y) + y + (\text{higher order terms of } y), \quad (10)$$

where $\gamma = 0.577\,21\ldots$ is Euler's constant. As can be seen from Eq. (9), all arguments of the exponential integral functions obey a standard, 1D diffusion scaling (length$^2 \sim$ time). Equation (10) shows that this scaling is dominant (the positive term "y"), but it also appears in the argument of a logarithmic function $[\ln(y)]$, which is a typical two-dimensional singularity. So the slab profiles are a "mixture" of typical 1D and 2D behaviors. The one-dimensional is asymptotically dominant, but there is a two-dimensional logarithmic correction, affecting primarily the short-time behavior, before the slab boundaries start to play a role in the kinetics.

In order to plot graphs of the theoretical profile functions in Eq. (9), we choose parameters that can be directly compared to the experimental data. The diffusion coefficient of the fluorescein in water is 4.37×10^{-10} m^2 s^{-1} [16]. Since each pixel in the experiment corresponds to 6.5×10^{-6} m, the diffusion constant is equivalent to 10.3 pixel^2 s^{-1}. This implies that Dt can be expressed in [pixel^2] by multiplying the time (seconds) by a factor of 10.3. Thus the times $t = 1, 11, 40, 160, 630, 1900$ (s) are equivalent to $Dt = 10, 113, 412, 1648, 6489, 19\,570$ (pixel^2) in Eq. (9). The total slab width is an order of 160 pixels, ranging from −80 (actually −77) to +80 (actually +77) pixels. Thus, in the following calculations we have substituted the $W = 160$ in Eq. (9). In addition, a numerical investigation of Eq. (9) indicates that the three terms $n = -1, 0, 1$ in the infinite series are actually sufficient for convergence, in most of the relevant parameter range.

In Fig. 6 we plot the parallel and perpendicular profiles, $P(x,t) = P(x, z=1; t)$ and $P(z,t) = P(x=1, z; t)$, respectively, for the above-mentioned parameters, in a time range of up to

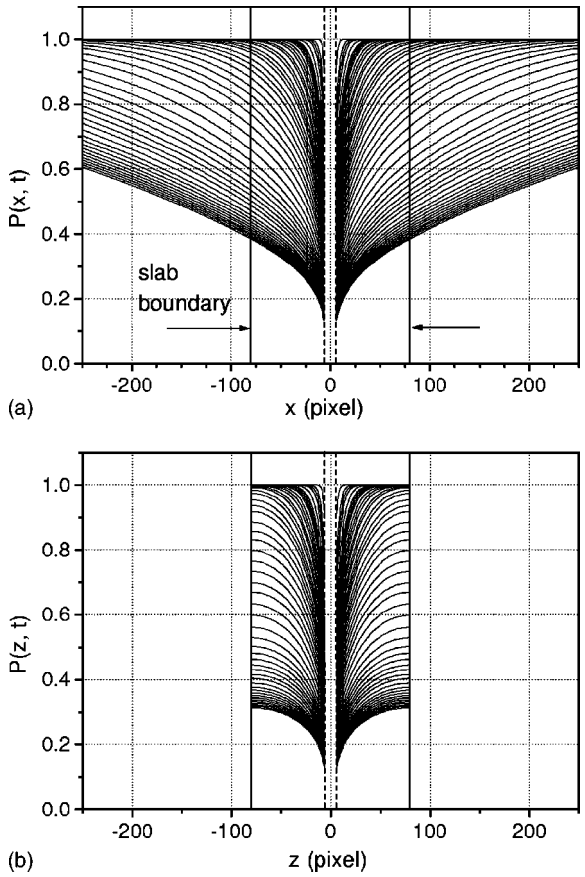

FIG. 6. Theoretical results of the concentration profiles along a pixel line (a) parallel, $P(x,t)$, and (b) perpendicular, $P(z,t)$, to the slab length, calculated using Eq. (9). The time range is from 1 s to 1900 s. The vertical solid lines represent the slab boundaries, while the vertical dashed lines represent the trap size in the experiment.

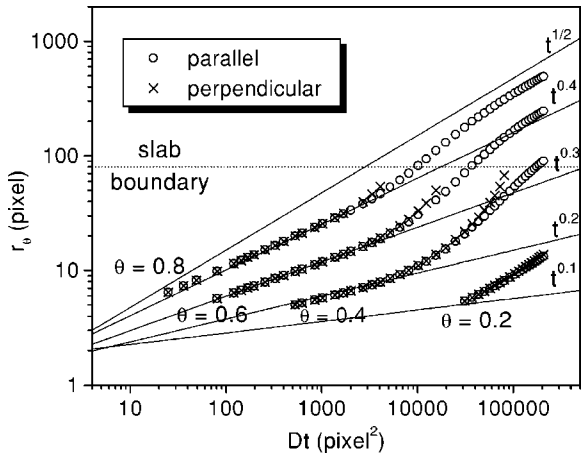

FIG. 7. The θ distance vs time for θ=0.2, 0.4, 0.6, and 0.8 from the theoretical data in Fig. 6. The circles represent the *parallel* θ distance measured from Fig. 6(a) and the crosses represent the *perpendicular* θ distance from Fig. 6(b). Both distances demonstrate a similar time scaling behavior for a given θ value until they reach the slab boundary, including a crossover from the initial 2D behavior ($t^{\theta/2}$) towards a 1D scaling ($t^{1/2}$).

1900 s, as in the experiments. This figure resembles remarkably well the corresponding experimental Fig. 4, having all the qualitative features discussed above. The vertical dashed lines in Fig. 6 represent the actual finite-sized boundaries of the trap. This is since the analytical expression [Eq. (9)] can only describe the concentration profile of the diffusing particles *outside* the trap. This has been discussed in detail in our earlier studies in two dimensions [2,3,11]. In Fig. 7 we plot the θ distances, similar to the experimental Fig. 5. They exhibit a very good agreement. Both θ distances start with 2D nonuniversal $t^{\theta/2}$, thereafter crossing over to the 1D $t^{1/2}$.

In order to gain better insight on the asymmetrical nature of the concentration profiles, we compare the two orthogonal profiles in Fig. 8. Figure 8(a) compares the experimental profiles, plotted using some selected profiles from Fig. 4, while Fig. 8(b) does the same for some theoretical curves plotted in Fig. 6. One can clearly see the effect of the boundary to diminish the perpendicular profile near the slab boundaries. This explains that our findings regarding the similar behavior of both θ distances measured from the trap result from the simple observation that the region where the perpendicular profile bends down is invisible to this depletion measure.

The vertical lines in Fig. 8 represent the actual trap size in the experiment. In the experimental system the trap radius

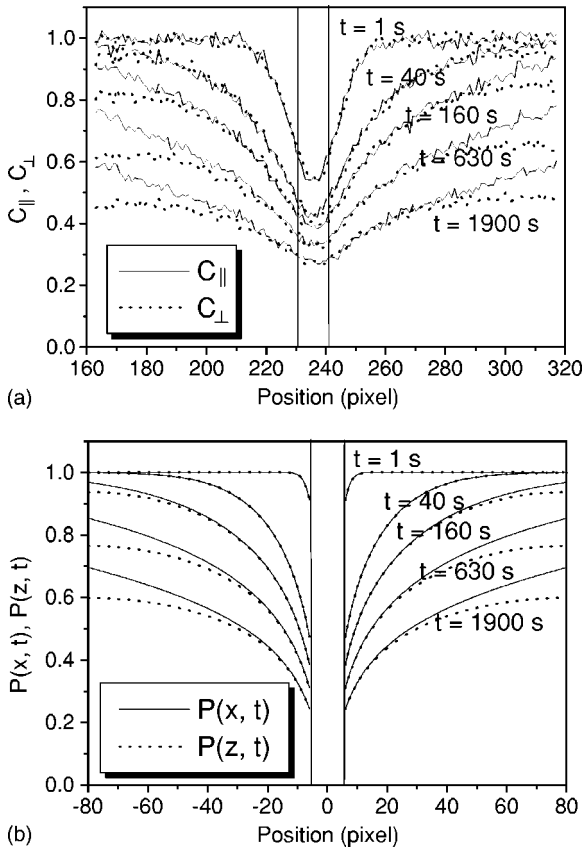

FIG. 8. The concentration profiles along a parallel (solid lines) and a perpendicular (dots) directions, plotted using some selected profiles at t=1, 40, 160, 630, and 1900 s from (a) the experimental curves in Fig. 4; (b) from the theoretical curves in Fig. 6. The vertical lines represent the actual trap size in the experiment.

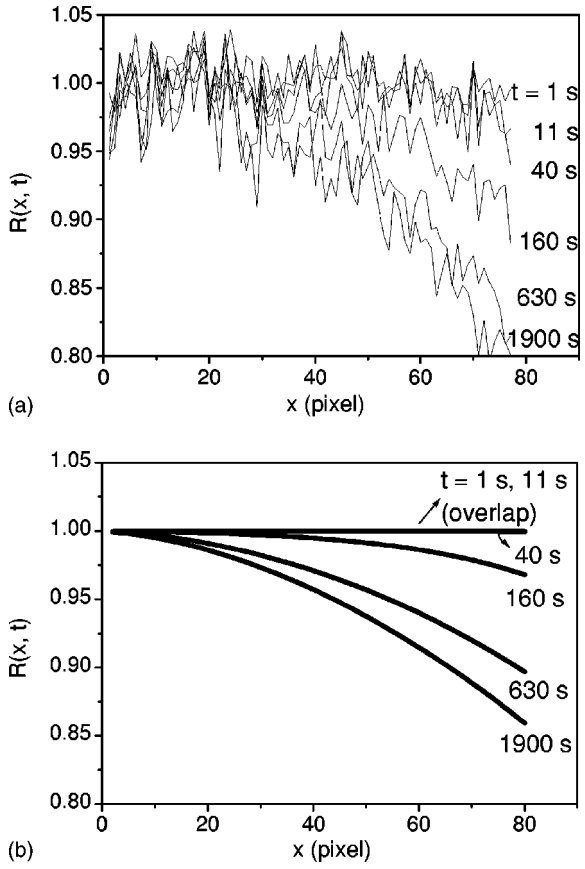

FIG. 9. The concentration profile ratios, $R(x,t)$, at $t=1$, 11, 40, 160, 630, and 1900 s for $W=160$ from (a) experiment and (b) theory.

(i.e., the laser beam width) is 5 pixels. The shape of the reactant concentration profile within this region has been discussed in detail in [2]. Nevertheless, the theoretical derivation, which assumes a point trap, agrees very well with the experimental profiles outside the finite-size trapping region.

It is interesting to compare the two orthogonal profiles through their ratio. Let us define the ratio, $R(x,t)$, as

$$R(x,t) = \frac{P(z=x,t)}{P(x,t)} \tag{11}$$

or, for the experimental system, as

$$R(x,t) = \frac{C_{\perp}}{C_{\parallel}}. \tag{12}$$

In Fig. 9, we plot the experimental (a), as well as the theoretical (b) ratios, for our system. It shows that, as time evolves, the deviation of the perpendicular profile from the parallel one increases. The agreement between the theoretical and the experimental ratios is evident.

The dimensional crossover of the depletion zone induced by the geometric confinement of the reaction space implies a crossover time that scales with the width of the reaction space. Previous work [13,14] has shown that the Einstein diffusion law correctly describes the crossover times for the onset of finite size effects in regular 1D, 2D, and 3D lattices.

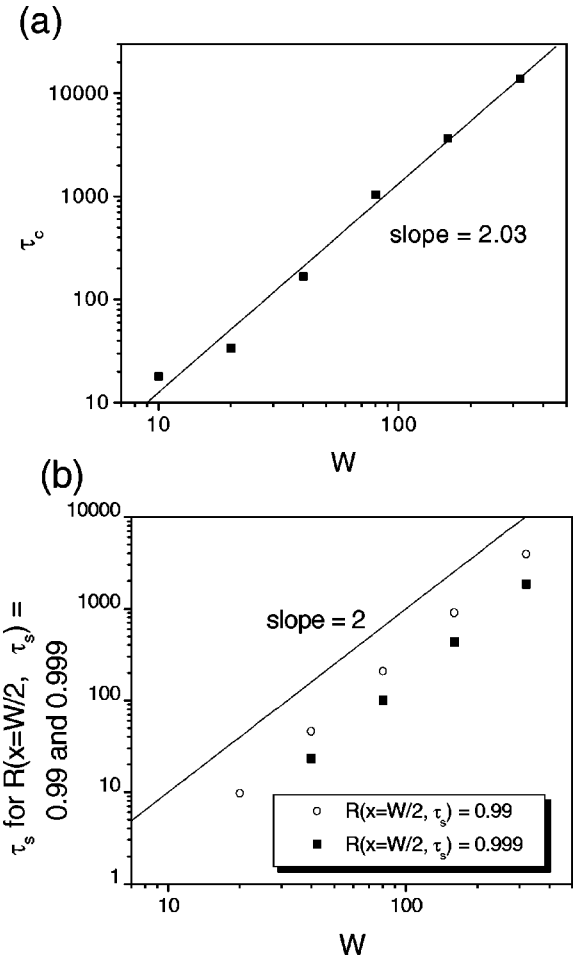

FIG. 10. (a) Crossover times, τ_c, for different slab widths at $W=10$, 20, 40, 80, 160, and 320, from the θ distances at $\theta=0.8$, measured from the theoretical curves similar to Fig. 6. (b) The time τ_s at which the ratio at the boundary, $R(x=W/2,\tau_s)$, is equal to 0.99 and 0.999, for several slab widths. The slopes confirm the Einstein diffusion law.

On the other hand, the Monte Carlo study [15] of the dimensional crossovers from 2D or 3D to 1D on baguette-like lattices for A+A and A+B reactions, with random initial condition, shows that the scaling of the crossover time with respect to the lattice width deviates significantly from the Einstein diffusion law and produces exponents ranging between 1 and 4, instead of an expected value of 2, depending on the lattice dimensionality and the reaction type. To determine if this law is relevant to the scaling of the crossover time against the width of the slab geometry, we must define the crossover time.

There are many different ways to determine the crossover time. One reasonable choice is the time when the θ distance has deviated from the two dimensional trajectory. The result for this choice, denoted by τ_c, is shown in Fig. 10(a) for several slab widths, as obtained from the theoretical expressions. The slope of 2.03 confirms the Einstein's Law prediction.

Another possible choice for the crossover time exploits our profile ratio analysis. One can look at the slab boundary distance $(x=W/2)$ for the time τ_s at which the ratio starts to

deviate from 1, i.e., where the perpendicular profile begins to split from the parallel concentration profile. This is shown in Fig. 10(b), where we have plotted the times τ_s at which the ratio at the boundary, $R(x=W/2,\tau_s)$, is equal to 0.99 and 0.999, for several slab widths W. Here again, as in Fig. 10(a), the slopes are around 2, as expected.

IV. SIMULATIONS

A. Methods

1. Monte Carlo simulations

Monte Carlo simulations were performed on a $201\times W$ ($W=5$, 7, 9, 11, 15, 21, 31, and 51) rectangular lattice, and a single point trap was put at the center of this lattice. Particles with an initial concentration $c_0=0.25$ are randomly generated on the lattice at a time step zero. No more than one particle is allowed to occupy a given site at any moment, i.e., we use the excluded volume principle. Particles are allowed initially to land both inside and outside the trap, randomly.

The diffusion is modeled by random walks of all particles, which are independent of each other. If a particle is chosen to move to a site that is already occupied by another particle, this move is not allowed and the particle remains at its original site for that time step. The trap is characterized by a trapping probability, p. This parameter p signifies the strength by which trapping may occur, and it varies from $p=0.0$ (no trapping at all) to $p=1.0$ (particle is always irreversibly trapped). Thus, each time that a particle moves into the trap site, the trapping probability p is compared to a new random number, leading to irreversible trapping (and removal from the system), or continuation of the diffusion process.

Cyclic boundary condition was used at the edges of the long dimension of the lattice, while reflective boundary condition was used at the edges of the short dimension of the lattice. However, we note that the cyclic and reflective boundary condition produce the same result in this particular case. The quantity monitored is the number of particles at a distance r from the origin (i.e., from the trap site). Since we use a discrete 2D lattice topology, the quantity $|i|+|j|$ is used as the value of r, for the position at (i,j) on the lattice. For a fixed time step, we count the total number of particles at each distance on the lattice. Then the number of particles is normalized into the concentration, using the total number of lattice sites at a given distance r, to measure the θ distance. The data are the average of 100 000 runs. For all simulations, the reactant profiles were followed from 1 up to 10 000 time steps.

2. Exact enumeration

We also ran exact enumeration using MATLAB. Similar to what we described previously [1–3], the principle is that, at any time, the concentration of any position is determined by the concentration of its nearest neighbors at the previous time step, that is, the concentration of any site on the square lattice at time t is one quarter of the sum of the concentrations of its four nearest neighbors at time step $t-1$. The boundary condition is reflective. In our previous work [1–3], we increased the size of the matrix for the concentration by one after each time step. In this work, in order to extend the time range, we increase the size of the concentration matrix only when the boundary values have 0.0001% change from the original value. By doing this, we can extend the time steps from 1000 to 50 000, which is needed to investigate the asymptotic regime, within a reasonable calculation time. As before, since the matrix size is not preset, we can consider that the lattice has an infinite length.

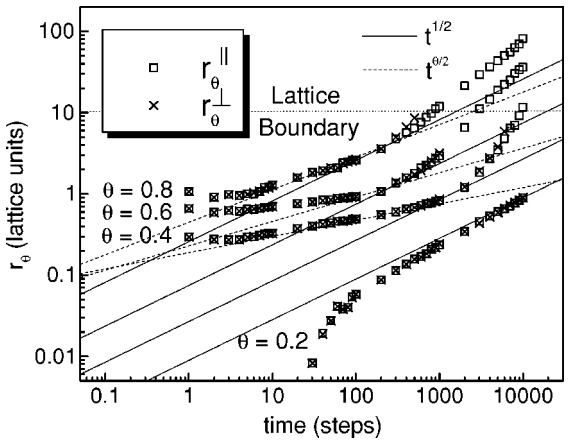

FIG. 11. The θ distance vs time at $\theta=0.2$, 0.4, 0.6, and 0.8 from a Monte Carlo simulation for a point trap system. The lattice size is 201×21 and a point trap with a trapping probability $p=0.5$ is located at the center of the lattice. The simulation data resemble well the experimental results shown in Fig. 5 and the theoretical results shown in Fig. 7.

B. Results

The Monte Carlo simulation results for a system of a point trap with a trapping probability $p=0.5$ on a 201×21 rectangular lattice are shown in Fig. 11. The θ distance shows almost perfect overlap between parallel and perpendicular directions for a given θ value in this figure, matching well with the experimental and theoretical results. At $\theta=0.4$, 0.6, and 0.8, the θ distance follows the previously observed [2,3] two-dimensional behavior for the time range up to ~200 steps, after which it experiences a sharp crossover to a higher slope, typical of a 1D-like behavior, just like the experimental results in Fig. 5 and the theoretical results in Fig. 7. At $\theta=0.2$, the θ distance starts with a two dimensional fast-growing, early-time behavior for the θ distances smaller than 1 lattice unit, which is the upper limit of the trap radius, and then switches directly to the one dimensional asymptotic behavior of $t^{1/2}$, without experiencing the previously observed (for the exact two-dimensional case) regime of slow growth [2,3]. This behavior is similar to the case for $\theta=0.4$ of the experimental results in Fig. 5.

It is worth pointing out that the slopes in the long time range in Fig. 11 are somewhat higher than the theoretically predicted asymptotic value of $\frac{1}{2}$ for the θ values at 0.4, 0.6, and 0.8, after the crossover from the two-dimensional behavior starts to happen. This is also consistent with the experimental and the theoretical results. As shown in Fig. 12(a), the

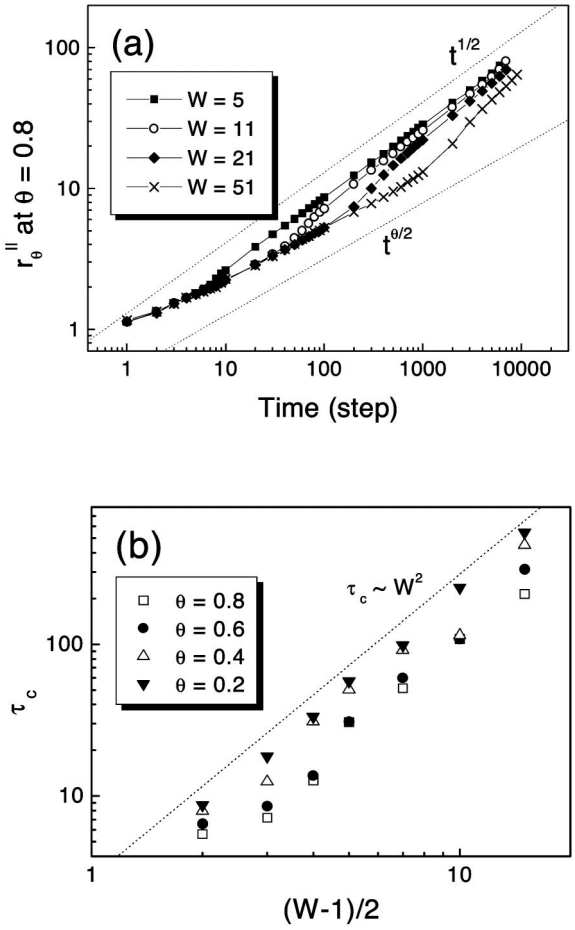

FIG. 12. (a) The θ distance in parallel direction vs time at $\theta=0.8$ from Monte Carlo simulations for a system with a perfect point trap located at the center of a two-dimensional rectangular lattice of size $201\times W$, with $W=5$, 11, 21, and 51. The deviation from two-dimensional behavior occurs later in time for a bigger lattice width. (b) Crossover time vs distance from the trap to the lattice boundary, $(W-1)/2$, for different lattice widths, at $\theta=0.2$, 0.4, 0.6, and 0.8. The crossover time scales as $\tau_c \sim W^2$, as expected from Einstein's diffusion law.

slope higher than $\frac{1}{2}$ seems to appear only temporarily, during the transition from 2D to 1D, according to the Monte Carlo simulations. This suggests that the theoretical 1D slope of $\frac{1}{2}$ should have eventually been recovered in Figs. 5 and 7, had the θ distance been monitored over a longer time range. The exact-enumeration results for the longer time range up to 50 000 time steps, as shown in Fig. 13, also clearly show the asymptotic 1D slope of $\frac{1}{2}$ for the θ distance along the parallel direction, as predicted.

In order to examine the width dependence of the dimensional crossover, Monte Carlo simulations were carried out for the point trap system on a 2D rectangular lattice with different lattice widths. Figure 12(a) shows the θ distance in time at $\theta=0.8$ from Monte Carlo simulations for a system with a perfect point trap located at the center of the two-dimensional rectangular lattice of size $201\times W$, where the width of the lattice W is varied over $W=5$, 11, 21, and 51. The two straight dashed lines represent the theoretical

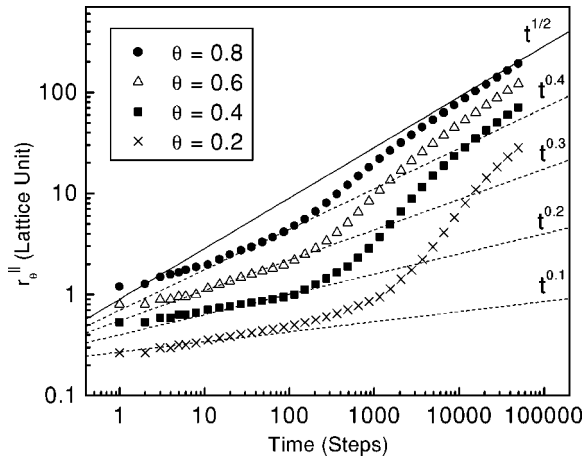

FIG. 13. The θ distance vs time at $\theta=0.2$, 0.4, 0.6, and 0.8 from exact enumeration for a point trap system. The lattice is infinitely long with a width of 15, and a point trap with a trapping probability $p=1$ is located at the center of the lattice.

asymptotic slope of $\frac{1}{2}$ for 1D and that of $\theta/2$ (i.e., 0.4 in this case) for 2D. A crossover from 2D to 1D occurs for all different widths. As mentioned earlier, it reproduces the transition slopes, higher than $\frac{1}{2}$, for all lattice widths, right after the onset of the crossover from the 2D to 1D behavior. These high slopes eventually converge to $\frac{1}{2}$ in the long time limit for the smaller widths at $W=5$ and 11, while for the bigger widths at $W=21$ and 51 they appear to approach the slope of $\frac{1}{2}$ towards covergence in later times. It also shows that the crossover occurs at different times for different widths. The crossover times, τ_c, measured as the point at which the θ distance has deviated from the two dimensional trajectory by a small fixed value (0.01 in this case) for $\theta=0.8$ from Fig. 12(a), as well as for other θ values of $\theta=0.2$, 0.4, and 0.6, are plotted in Fig. 12(b) against the distance from the trap to the lattice boundary, $(W-1)/2$. The crossover times do scale

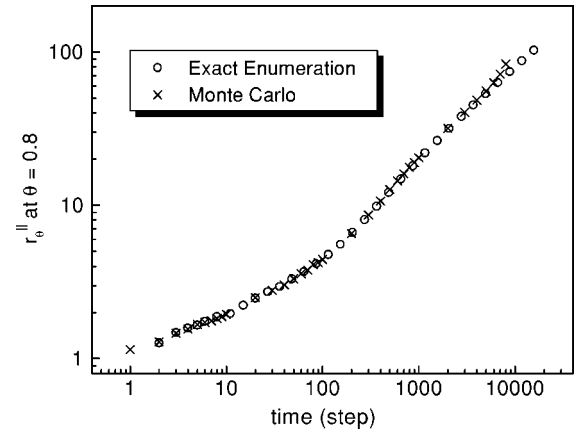

FIG. 14. The θ distance at $\theta=0.8$ in parallel direction vs time for a slab width $W=15$ from the exact enumerations (○) and the Monte Carlo simulations (×). A point trap with a trapping probability $p=1$ is located at the center of the lattice. The data from the two approaches agree with each other very well, over the entire time range, thus suggesting that any potential correlated diffusion effects in the Monte Carlo calculations are negligible.

simply as $\tau_c \sim W^2$, suggesting that the Einstein diffusion law, with respect to the width of the slab geometry, is relevant to the scaling of these crossover times for the growth of depletion zones around a trap.

The use of the excluded volume principle, combined with an initial concentration as high as 0.25, may suggest the possibility of correlated diffusion effects in our Monte Carlo simulations. Such a possibility can be tested by comparing the results from the Monte Carlo calculations with those from the exact enumeration method, as the latter should not exhibit any correlation effects. The comparison is shown in Fig. 14. It shows that the θ distances in the parallel direction at $\theta=0.8$, for a slab width $W=15$, derived from the two different approaches, do agree very well over the entire time range. (Only a small deviation occurs at a θ distance near 100, which is at the boundary of the 201×15 square lattice in the Monte Carlo calculation, where the extra depletion occurs as explained above.) This result strongly suggests that any possible correlated diffusion effects are absent, or at least negligible, in the presented Monte Carlo calculations.

V. SUMMARY

We present the study of the growth of a depletion zone around a single point trap located in the middle of a flat microchannel having a slab geometry, using various methods: experiment, theory, Monte Carlo simulation, and exact enumeration. We observe how the θ distance scales with time in two orthogonal directions, parallel with and perpendicular to the long axis of the slab, as the reaction progresses. At the very beginning, the θ distance scales anomalously as $t^{\theta/2}$, as expected for 2D geometry. Then, when the particles feel that the system is not strictly two dimensional, the θ distances in both parallel and perpendicular directions deviate from $t^{\theta/2}$. The crossover time is proportional to the square of the slab width, according to Einstein's diffusion law. The θ distance in the perpendicular direction increases faster than the counterpart in the parallel direction. This is because of the diminished supply of particles to the regions very close to the boundary. At last, after a region of faster increase of θ distance (the power is greater than $\frac{1}{2}$), the θ distance finally scales with $t^{1/2}$ as we would expect from 1D geometry. The ratio of the concentration profiles in the two orthogonal directions provides another means to look at the crossover characteristics in this restricted, low-dimensional geometry. Our experimental, theoretical and numerical methods agree very well with each other.

ACKNOWLEDGMENT

Support from NSF Grant No. DMR 9900434 is gratefully acknowledged.

[1] S. H. Park, H. Peng, S. Parus, H. Taitelbaum, and R. Kopelman, J. Phys. Chem. A **106**, 7586 (2002).
[2] S. H. Park, H. Peng, R. Kopelman, P. Argyrakis, and H. Taitelbaum, Phys. Rev. E **67**, 060103(R) (2003).
[3] H. Peng, S. H. Park, P. Argyrakis, H. Taitelbaum, and R. Kopelman, Phys. Rev. E **68**, 061102 (2003).
[4] A. A. Ovchinnikov and Y. B. Zeldovich, Chem. Phys. **28**, 215 (1978).
[5] A. Blumen, J. Klafter, and G. Zumofen, Phys. Rev. B **28**, R6112 (1983).
[6] R. Kopelman, Science **241**, 1620 (1988).
[7] G. H. Weiss, R. Kopelman, and S. Havlin, Phys. Rev. A **39**, R466 (1989).
[8] H. Taitelbaum, R. Kopelman, G. H. Weiss, and S. Havlin, Phys. Rev. A **41**, 3116 (1990).
[9] S. Redner and D. Ben-Avraham, J. Phys. A **23**, L1169 (1990).
[10] S. Havlin, H. Larralde, R. Kopelman, and G. H. Weiss, Physica A **169**, 337 (1990).
[11] H. Taitelbaum, Phys. Rev. A **43**, 6592 (1991).
[12] K. Lindenberg, P. Argyrakis, and R. Kopelman, J. Phys. Chem. **99**, 7542 (1995).
[13] A. Lin, R. Kopelman, and P. Argyrakis, Phys. Rev. E **53**, 1502 (1996).
[14] P. Argyrakis, R. Kopelman, and K. Lindenberg, Chem. Phys. **177**, 693 (1993).
[15] A. L. Lin, R. Kopelman, and P. Argyrakis, Phys. Rev. E **54**, R5893 (1996).
[16] P. H. Paul, M. G. Garguilo, and D. J. Rakestraw, Anal. Chem. **70**, 2459 (1998).
[17] H. S. Carslaw and J. C. Jaeger, *Conduction of Heat in Solids*, 2nd ed. (Oxford University Press, Oxford, 1959), Sec. 14.10.